ICJK
Journal of Carbon Neutrality
http://dx.doi.org/10.62762/JCN.2026.937655

RESEARCH ARTICLE

Numerical Study of Premixed Hydrogen/Air Flame-Wall Interaction for Confined Systems

Ziyin Chen[1,*] **and Yuxi Mai**[2]

[1] Aix Marseille Univ, CNRS, Centrale Med, M2P2, Marseille, France
[2] School of Management, Northwestern Polytechnical University, Xi'an 710072, China

Abstract

Accurate modeling of flame-wall interaction is essential for predicting premixed hydrogen combustion in confined configurations relevant to hydrogen-based energy systems. Detailed chemical mechanisms often produce unphysical near-wall heat release due to persistent radical-consuming reactions at low temperatures, reducing simulation fidelity and limiting predictive capability. To address this, we apply an H radical recombination model that selectively removes H radicals at the wall through recombination to H_2 while conserving mass. The model is validated using canonical flame-wall interaction scenarios, including head-on quenching of stoichiometric hydrogen/oxygen flames and side-wall quenching of premixed hydrogen/air flames. One- and two-dimensional simulations evaluate flame propagation, quenching, and stability with isothermal walls. Results show that H radicals dominate abnormal near-wall heat release, and selective recombination effectively suppresses this behavior. In side-wall quenching, the model reproduces experimental flame propagation speed accurately. For wider channels, wall heat losses destabilize asymmetric flames and promote symmetric configurations, consistent with experiments. This H radical recombination model provides a physically consistent and computationally efficient strategy for capturing flame-wall interactions and heat losses in premixed hydrogen flames. By improving near-wall prediction fidelity in confined configurations, it supports more reliable simulations of hydrogen combustion systems, advancing the development of safe and efficient carbon-neutral energy technologies.

Keywords: hydrogen combustion, flame-wall interaction, confined flames, wall heat losses, numerical modeling.

1 Introduction

Interest in hydrogen has increased significantly over the past decade due to its potential as a carbon-neutral fuel and energy carrier, making it a promising candidate for mitigating global warming. However, hydrogen is characterized by a wide flammability range and high chemical reactivity. While these properties are advantageous for lean combustion applications, they also make hydrogen flames particularly prone to interacting with solid boundaries. As a result, hydrogen

Submitted: 13 February 2026
Accepted: 06 May 2026
Published: 12 May 2026

Vol. 1, **No.** 1, 2026.
10.62762/JCN.2026.937655

***Corresponding author:**
✉ Ziyin Chen
ziyin.chen@univ-amu.fr

Citation
Chen, Z., & Mai, Y. (2026). Numerical Study of Premixed Hydrogen/Air Flame-Wall Interaction for Confined Systems. *Journal of Carbon Neutrality*, 1(1), 29–37.

flames tend to propagate closer to walls and induce higher thermal loads compared to hydrocarbon flames, highlighting the importance of understanding flame-wall interaction (FWI) [1]. FWI is a complex and transient phenomenon that strongly influences flame structure, near-wall heat transfer, and radical quenching, and plays a critical role in the performance, durability, and safety of wall-bounded combustion systems.

Three canonical configurations have been extensively investigated to study FWI, both experimentally and numerically [1]. These include head-on quenching (HOQ), in which a flame propagates directly toward a wall; side-wall quenching (SWQ), where the flame propagates parallel to a solid surface; and tube quenching (TQ), in which the flame interacts with the walls of a confined duct or channel. Each configuration captures different aspects of near-wall flame behavior and provides valuable insight into quenching mechanisms relevant to practical combustion devices.

Accurate modeling of hydrogen combustion generally requires the use of detailed chemical reaction mechanisms. However, when applied near cold walls, conventional detailed mechanisms often lead to the artificial accumulation of intermediate species and radicals. In particular, an abnormal increase in heat release rate is frequently observed in the near-wall region [3]. For instance, previous studies have reported that conventional mechanisms can overpredict the wall heat flux by up to 30% due to the artificial accumulation of reactive radicals near the wall [2]. This behavior is mainly attributed to low-activation-energy, weakly temperature-dependent reactions that continue to consume radicals and generate intermediate species despite the low temperatures typically encountered close to the wall. In contrast, experimental measurements consistently report near-zero radical mass fractions in the vicinity of cold surfaces [4], indicating a clear discrepancy between numerical predictions and physical observations. Moreover, recent numerical studies have identified discrepancies between predicted and experimentally observed first and second explosion limits of H_2/O_2 mixtures when specific wall treatments are not included, namely the fitting of wall sticking coefficients [5, 6]. These findings highlight the importance of incorporating wall treatments in CFD, rather than relying on the commonly assumed inert wall conditions.

Several modeling strategies have been proposed to mitigate this numerical issue, including the incorporation of surface reaction and catalytic wall models. While these approaches can reduce excessive wall heat fluxes, they are often associated with increased computational cost and modeling complexity [7]. Popp and Baum [2] demonstrated that removing H, O, and OH radicals at the wall can reduce the wall heat flux by approximately 30%, with H identified as the dominant contributor to near-wall heat release. However, this approach violates mass conservation. Instead, Peters and Warnatz [4] proposed an H radical recombination model (2H $\rightarrow$ H_2), which was shown to provide accurate predictions of wall heat flux in burner-stabilized, stoichiometric hydrogen/air premixed flames while preserving mass conservation. Despite its promising performance, the applicability and impact of the H radical recombination strategy in confined flame-wall interaction scenarios remain insufficiently explored. Moreover, wall heat losses and near-wall chemical processes can strongly alter flame stabilization, propagation, and symmetry in confined and compact combustion devices. In particular, flame symmetry is a key factor for operational safety, as asymmetric flames may be destabilized by heat losses and transition to symmetric configurations, which exhibit different propagation dynamics [8, 9]. Understanding the mechanisms governing flame symmetry and stability in confined hydrogen combustion is therefore essential for the safe and reliable design of next-generation hydrogen-based energy technologies.

Regarding flame symmetry stability confined between two walls, previous work in [10] demonstrated that, under adiabatic wall conditions, hydrogen flames exhibit multiple solution branches. For channel widths h exceeding a critical value $L_{z,NS}$, at least one asymmetric half-hump solution exists. When h exceeds a critical value h_c, a stable symmetric solution also emerges, which subsequently destabilizes into an asymmetric one-hump flame with further increases in h, while the asymmetric half-hump solution persists. The final flame configuration depends strongly on the initial conditions. Notably, the symmetric flame branch predicted numerically under adiabatic conditions has not been observed experimentally, suggesting that wall heat losses may play a decisive role in suppressing certain solution branches and stabilizing flame symmetry.

In parallel, the influence of wall heat losses on flame symmetry and stability has been examined

using two-dimensional configurations. Studies have shown that wall heat losses can destabilize asymmetric flame fronts and promote symmetric flame shapes[8, 9]. However, most existing investigations rely on simplified chemical kinetics or focus on hydrocarbon fuels, whereas the symmetry behavior of hydrogen flames under realistic heat-loss conditions remains poorly understood. Moreover, the influence of wall heat losses on flame surface evolution, flame speed, and shape transition has not been systematically addressed for hydrogen combustion.

Motivated by the need to improve predictive fidelity for hydrogen combustion in confined and wall-bounded configurations, the present study investigates premixed hydrogen/air flame-wall interaction using an H radical recombination model. Particular emphasis is placed on suppressing abnormal near-wall heat release rate predicted near cold walls when using detailed chemical mechanisms and elucidating the role of wall heat losses in flame symmetry, stability, and safety-relevant behavior.

2 Methodology

2.1 Governing formulation

The mass, momentum, energy, and species equations are solved in conservative form using the Lattice-Boltzmann solver ProLB [10–12]. For a detailed derivation of the numerical method, the reader is referred to [13].

The mass and momentum equations are in the following forms:

$$\begin{aligned} &\frac{\partial \rho}{\partial t} + \nabla \cdot [\rho \mathbf{u}] = 0 \\ &\frac{\partial \rho \mathbf{u}}{\partial t} + \nabla \cdot [\rho \mathbf{u}\mathbf{u}] = -\nabla p + \nabla \cdot \mathcal{T} \end{aligned} \tag{1}$$

where ρ is the density, $\mathbf{u}$ is the flow velocity, p is the pressure and $\mathcal{T}$ is the viscous tensor. The conservation of species is considered as:

$$\frac{\partial \rho Y_k}{\partial t} + \nabla \cdot [\rho \mathbf{u} Y_k] = \nabla \cdot (-\rho V_k Y_k) + \dot{\omega}_k \tag{2}$$

where Y_k is the mass fraction of species k, $\dot{\omega}_k$ is its reaction rate. V_k stands for the diffusion velocity, which can be evaluated through Fickian approximation:

$$V_k = -D_k \nabla \ln Y_k + V_c, \tag{3}$$

with V_c the correction velocity to ensure a zero total mass diffusion, i.e. the mass conservation. It can be evaluated as:

$$V_c = \sum_{j=1}^{N} \frac{D_j}{Y_j} \nabla Y_j. \tag{4}$$

The energy conservation can be represented by various forms such as the total energy, the internal energy, etc. In our fully-compressible case, it is expressed in the form of total energy (E_t), as following:

$$\frac{\partial \rho E_t}{\partial t} + \nabla \cdot [\rho \mathbf{u} E_t] = -\nabla q + \nabla \cdot [(\mathcal{T} - pI)\mathbf{u}] \tag{5}$$

with

$$\begin{aligned} E_t = \sum_{k=1}^{N} Y_k e_{t,k},\ e_{t,k} = \int_{T_0}^{T} C_{v,k}(T)\mathrm{d}T - \frac{RT_0}{W_k} \\ + \Delta h^o_{f,k} + \frac{1}{2}\mathbf{u}\cdot\mathbf{u} \end{aligned} \tag{6}$$

where I is the identity matrix. $C_{v,k}$ is the species heat capacity at constant volume, the reference temperature is at $T_0 = 300\,\mathrm{K}$, and $\Delta h^o_{f,k}$ is the species mass formation enthalpy. For the heat energy flux q, we have:

$$q = -\lambda \Delta T + \rho \sum_{k=1}^{N} h_k Y_k V_k \tag{7}$$

where λ is the thermal conductivity and $\lambda = \frac{\mu C_p}{Pr}$ with μ the dynamic viscosity. Pr is the Prandtl number. Ideal gas equation of state $\frac{\rho RT}{W} = p$ is commonly applied for thermodynamic closure with the perfect gas constant $R = 8.314\,\mathrm{J/molK}$.

The flow is considered as an ideal gas and a 12-step skeletal hydrogen/air mechanism is considered [14, 15]. Transport properties are calculated assuming constant Prandtl number ($Pr = 0.75$) and species-specific Schmidt numbers for fresh gases (Sc_k, H_2: 0.21, H: 0.14, O_2: 0.8, OH: 0.53, O: 0.53, H_2O: 0.6, HO_2: 0.8, H_2O_2: 0.82, N_2: 1.0). These parameters are those recommended in Cerfacs' database [16] and validated for this mechanism.

The domain is initially filled with premixed mixtures at a temperature $T_\infty = 300\,\mathrm{K}$ and pressure $p = 1\,\mathrm{bar}$. The laminar thermal flame thickness is defined as $\delta_T = (T_b - T_u)/max(|\nabla T|)$. A constant pressure outlet at 1 bar is applied on the burnt side, formulated as

$$x \longrightarrow -\infty : \frac{\partial \mathbf{u}}{\partial x} = \frac{\partial T}{\partial x} = \frac{\partial Y_k}{\partial x} = 0 \tag{8}$$

A non-reflecting boundary condition is applied on the fresh side, see [1].

2.2 Configuration

Head-on quenching

For head-on quenching problem, a one-dimensional domain of length $L_x = 10\,\mathrm{mm}$ filled with quiescent premixed hydrogen/oxygen mixtures at stoichiometric ratio is set, with an outlet for burnt gases at constant ambient pressure $P_{out} = P_0$ on the right hand side. While a non-slip cold wall on the left hand side is set at fresh gases temperature $T_w = 300\,\mathrm{K}$. The flame propagates toward the wall at a constant speed S_L. The grid size is set to $\Delta x = \delta_T/22 = 1 \times 10^{-5}\,\mathrm{m}$. Figure 1 provides the sketch of the setup. It should be mentioned that the laboratory (fixed) reference frame is used, because it is the transient regime that we want to study.

Figure 1. Sketch of 1D configuration for HOQ.

Side-wall quenching

For side-wall quenching problem, the geometrical configuration is shown in Figure 2. The domain length L_x is set at 10 times longer than the channel width h. The grid size is set to $\Delta x = 1 \times 10^{-5}\,\mathrm{m}$ for an accurate resolution near the wall. The boundary conditions along the longitudinal direction are set as the same: a constant pressure outlet for burnt gases on the left hand side and a non-reflecting inlet for fresh gases on the right hand side. While the top and bottom non-slip cold walls are set at $T_w = 300\,\mathrm{K}$. Premixed hydrogen/air flames propagate from left to right. A reference frame attached to the flame is applied to reduce the computational cost, with a speed at the flame consumption rate $\mathbf{U}_{ref} = \{S_c, 0, 0\}$, and S_c is defined as

$$S_c = -\frac{1}{\rho_u Y_{D,u} h L_y} \int_0^{L_x} \int_0^{L_y} \int_0^{h} \dot{\omega}_D \mathrm{d}x\mathrm{d}y\mathrm{d}z \qquad (9)$$

where D stands for the deficient fuel in fresh mixtures and $\dot{\omega}_D$ is the fuel consumption rate. ρ_u and $Y_{D,u}$ are the density and the deficient fuel mass fraction of the unburnt mixture.

Initially, the simulation is carried out in the laboratory reference frame, but once the flames reach halfway, the reference frame of the flame is used so that the flame remains close to the center for the remainder of the simulation. The transient time before reaching a stable flame front shape varies with the equivalence ratio and channel width, but the simulation is carried out until convergence.

A grid convergence test has been conducted with two mesh sizes: $\Delta x = 1 \times 10^{-5}\,\mathrm{m}$ (coarse) and $\Delta x = 0.5 \times 10^{-5}\,\mathrm{m}$ (fine).The stoichiometric hydrogen/oxygen premixed flame is chosen for the convergence test given its much thinner flame thickness compared to hydrogen/air premixed flames. The temperature profiles of freely propagating stoichiometric premixed hydrogen/oxygen flames are shown in Figure 3 for the two grids. No observable difference is noticed between two cases. Moreover, the deviation between maximum HRR, calculated as

$$|\Delta HRR| = \frac{|max\{HRR_{coarse}\} - max\{HRR_{fine}\}|}{max\{HRR_{fine}\}},$$

is less than 0.5%. Hence, the flame configuration is well resolved with the chosen grid $\Delta x = 1 \times 10^{-5}\,\mathrm{m}$.

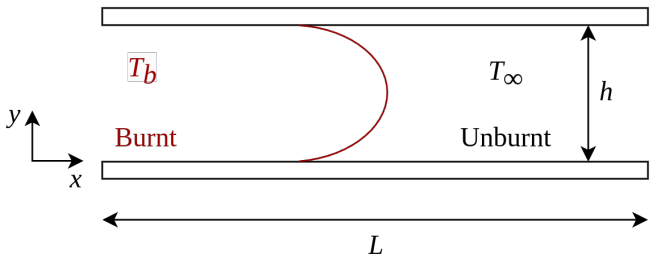

Figure 2. Sketch of asymmetric flame propagating from left to right in the thickness of a Hele-Shaw cell with a gap size h.

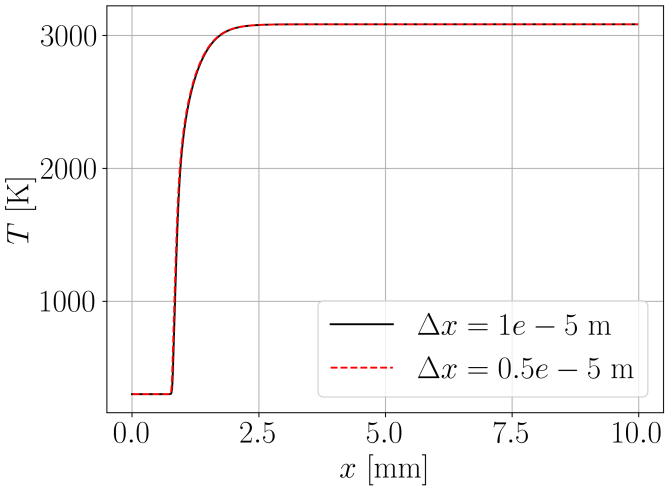

Figure 3. Temperature profile of freely propagating stoichiometric hydrogen/oxygen flames at two grid sizes.

2.3 Wall treatment

Here, two wall treatments are tested:

1 - Inert wall.

2 - 2H $\longrightarrow$ H_2

to investigate the primary responsible species for the explosive heat release rate (HRR) on the wall, and tested through two configurations: HOQ and SWQ. Note that for inert wall, a zero-flux (Neumann) boundary condition is applied for all species; while for wall with H-recombination treatment, the Neumann condition still applies to all species except for H and H_2.

3 Results and discussion

3.1 Head-on quenching

First the flame structures are investigated with the two wall treatments. The distribution of temperature is plotted in Figure 4 for several instants: t_0 signifies the instant of flame reaching the wall, and $\Delta t = 5.7735 \times 10^{-6}\,\mathrm{s} = 0.23 t_c$, with the flame characteristic time $t_c = \delta_T / S_L$. A negligible difference is observed between the two wall treatments.

Besides, the distribution of HRR (normalized by the maximum HRR value of free propagating laminar flame) before flame reaching the wall is also the same for the two cases. However, a significant discrepancy is found in comparing the HRR for $t \geq t_0$, as shown in Figure 4(b). At t_0, an explosive increase of HRR occurs near the wall, and the maximum value is located at the wall, which decreases gradually with time. On the other hand, H radical recombination model suppresses the unphysical increase of HRR. Moreover, the maximum of HRR occurs on the second node near the wall at $t \geq t_0$, and a negligible HRR is observed on the wall due to the accumulation of other intermediate radicals (O, OH, $etc.$). For $t \geq t_0$,HRR drops eventually to near zero, as expected. A comparison of the computation cost is conducted for inert walls and walls with H recombination model. Starting from a given distance to the wall ($1 \times 10^{-3}\,\mathrm{m}$), both simulations were carried out using the same grid, solver settings and number of CPUs (20), ensuring that flame-wall interaction occurs in both cases. For a total number of iterations (6×10^5), the total wall-clock time is 45 s for the baseline case (inert wall), and 46 s for the case with the H radical recombination model, corresponding to a difference of approximately 2%.

It is then concluded that H radical recombination model can efficiently decrease the heat release rate at the cold wall. Besides, the H radical turns out to be the crucial intermediate species for the explosive heat release rate.

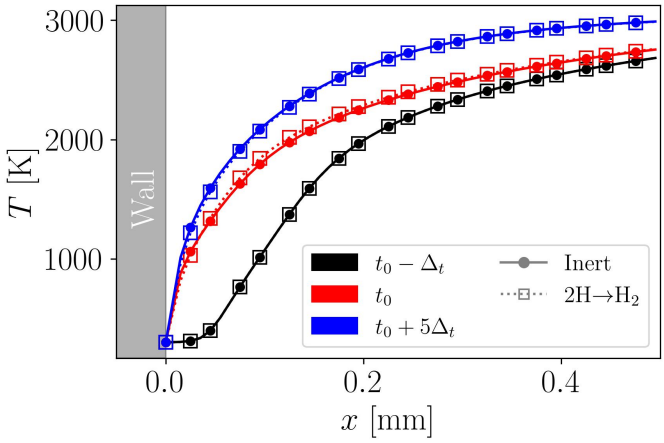

(a)

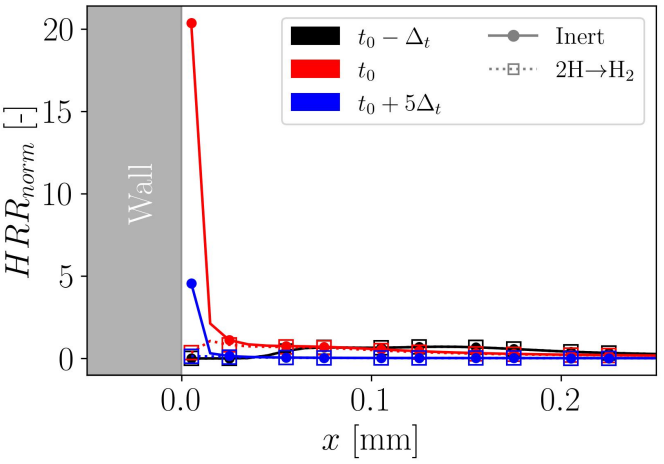

(b)

Figure 4. Evolution of temperature (a) and HRR (b) w/o H radical on the wall.

3.2 Side-wall quenching

To investigate side-wall quenching, a premixed hydrogen/air mixture at $\phi = 1.2$ is considered and ignited between two isothermal walls separated by a channel width of $h = 0.56\,\mathrm{mm}$. The flame eventually reaches a steady state, propagating at a constant speed with a symmetric structure. The distribution of HRR for inert walls is shown in the upper part of Figure 5. The colormap corresponds to the colorbar in the upper left, indicating the range of normalized heat release rate. It can be observed that $HRR_{norm} \leq 1$ over most of the domain, except in the near-wall region where higher values are observed.

A zoomed-in view near the top wall is presented in the subplot, where the mesh configuration is explicitly shown. A sharp increase in HRR is observed at the first layer of nodes adjacent to the wall, with the maximum value indicated by a green solid star. In

Table 1. Characteristic parameters at various wall treatments for $\phi = 1.2$ and $h = 0.56\,\mathrm{mm}$.

Wall treatment	$\max(HRR_{norm})$ $[-]$	$\max(T)$ [K]	S_c [m/s]
Inert	12.11	1511	1.854
2H$\rightarrow$ H_2	0.65	1471	1.375

contrast, when the H radical recombination model is applied, the maximum HRR is significantly reduced to below 0.7 and shifted to the second node layer away from the wall, which is also marked by a star, as shown in the lower part of Figure 5. A different colormap is used for this case to improve visualization, corresponding to the colorbar in the lower left.

Note that the flame reactivity near wall is higher than the center region. This near-wall behavior is influenced by preferential diffusion, which enhances local reactivity in regions of negative curvature near the wall, associated with an effective Lewis number slightly above unity.

A quantitative comparison is presented in Table 1. Compared to the H radical recombination model, the inert wall not only exhibits a much higher maximum HRR at the wall but also results in higher peak temperature and flame consumption speed. The H radical recombination model, however, recovers flame speeds consistent with experimental data [17], further supporting the conclusion that H radicals are primarily responsible for the abnormal near-wall phenomena.

Furthermore, the SWQ configuration allows for an investigation of flame propagation and quenching limits. As reported in our previous study [17], the flame propagation speeds and quenching limits show good agreement with experimental observations, while the inert walls largely overpredict the flame speed, as shown in Figure 6, which shows the evolution of flame consumption speed with the channel width.

3.3 Impact of heat losses on flame symmetry

To investigate solution multiplicity and stability under heat losses at larger channel widths, $\phi = 0.43$ and $h = 1.56\,\mathrm{mm}$ are chosen as representative mean mixtures. Since $h > h_c$, two stable adiabatic solutions exist: a half-hump asymmetric and a one-hump symmetric flame. The top row of Figure 7 shows the normalized hydrogen reaction rate, $\dot{\omega}_{\mathrm{H_2}}$, for steady solutions initialized with planar (top left) and hot spot (top right) conditions without heat losses. Red contours indicate the flame front at $T = 1000\,\mathrm{K}$. The two cases are numbered I and III.

A zoom near the wall of case I reveals that, with adiabatic walls, the maximum H_2 reaction rate occurs at the top wall in the asymmetric one-hump shape, due to the Lewis number effect on the positive flame front curvature. Conversely, the strongly concave flame front near the bottom wall yields negligible reaction rates. For further insights, Figure 8 presents the local atom-based equivalence ratio, ϕ_{atom} of case I and III, with

$$\phi_{atom} = \frac{Y_H/Y_O}{\{Y_H/Y_O\}_u}.$$

For both asymmetric and symmetric cases, preferential diffusion leads to an enrichment of the local equivalence ratio in convex regions and a depletion in concave regions. As shown in Figure 8(a), the local ϕ_{atom} in the upper part of the flame front increases from the inlet value of 0.43 up to approximately 0.53 due to strong convex curvature. In contrast, ϕ_{atom} in the lower part decreases to about 0.21, which reduces local flammability and explains the weak reaction rate observed in case I of Figure 7(a), even in the absence of wall heat losses.

A similar trend is observed for the symmetric case in Figure 8(b), where ϕ_{atom} ranges from approximately 0.24 to 0.50. The enrichment occurs in the convex central region, while depletion takes place in the concave regions near the upper and lower walls, contributing to flame weakening and eventual extinction in near-wall regions.

The isothermal walls are then set to integrate the heat losses at walls. Initialized with the two steady solutions with adiabatic walls, the isothermal walls lead to steady symmetric solutions, as shown in bottom row in Figure 7. The two cases are numbered II and IV. With heat losses, the reaction rate on the top wall vanishes and the asymmetric flame loses its stability and converts into symmetric shape. However, if the initialized with symmetric solution with adiabatic walls, which already shows weak reaction near the top and bottom walls because of the preferential diffusion, the symmetric flame shape is stable toward the heat losses and sustain the symmetric shape.

The flame front surface and consumption speeds for the four cases are summarized in Table 2. For case II which is initialized with the asymmetric solution, the loss of asymmetry significantly reduces the flame front surface and, consequently, the consumption speed compared to case I. Interestingly, heat losses have a relatively minor effect on consumption speed from case III to IV (a reduction of approximately

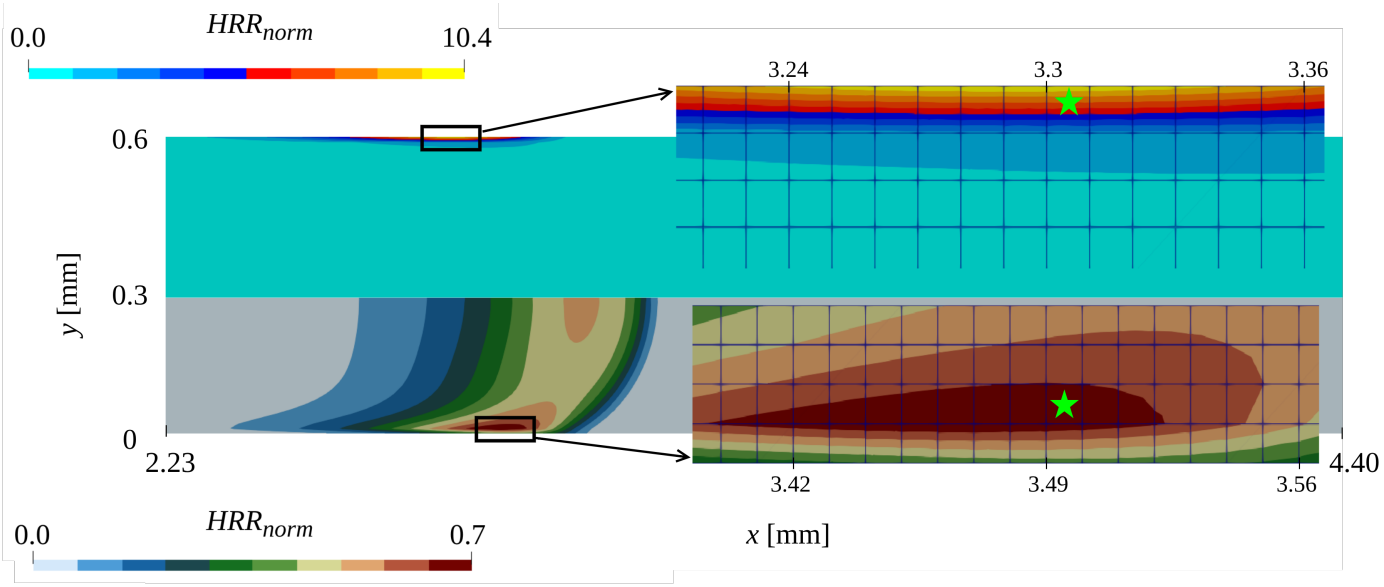

Figure 5. HRR for inert isothermal walls (up) and walls with H recombination model (bottom) at $h = 0.56\,\mathrm{mm}$. The subplots show zoom-in views of the near-wall regions, where the mesh configuration is explicitly displayed. The locations of maximum HRR are indicated by green star markers.

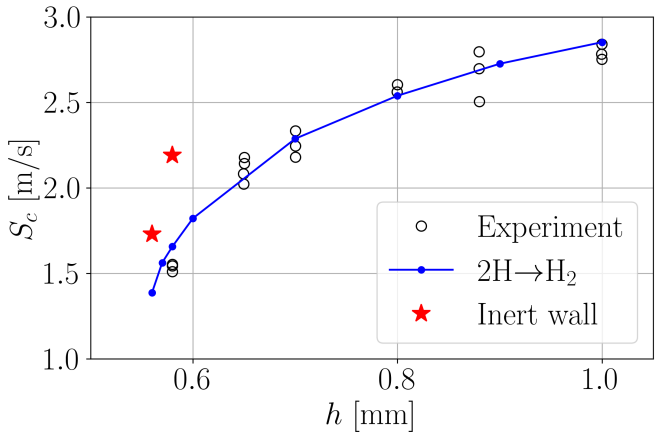

Figure 6. Evolution of flame consumption speeds S_c with channel widths h.

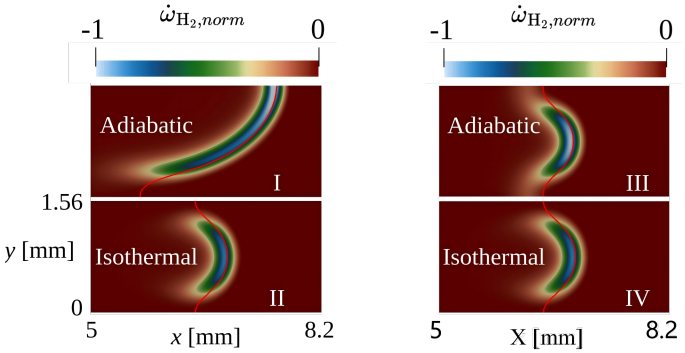

(a) Planar initial condition

(b) Circular initial condition

Figure 7. $\phi = 0.43$, $h = 1.56\,\mathrm{mm}$, adiabatic (top row) and isothermal walls (bottom row).

3%), which is attributed to the very low reaction rate near the adiabatic walls. The amplification factor, $I_0 = \{S_c/S_L\}/\{A_0/A_f\}$, is also listed to quantify the Lewis number effect on local curvature. For the adiabatic half-hump asymmetric flame (case I), I_0 is larger than for the adiabatic symmetric flame (case III). Introducing heat losses (case III to IV) slightly reduces both A_f and I_0, while cases II and IV are effectively identical. Overall, these results indicate that heat losses have a limited impact on symmetric lean hydrogen-air flames.

With further increases in channel width, as discussed in [10] for adiabatic walls, one-hump asymmetric flame fronts in simulations are often more asymmetric than observed experimentally, and some flames that

Table 2. Characteristic parameters at various wall boundary conditions for $\phi = 0.43$ and $h = 1.56\,\mathrm{mm}$.

Parameter	I	II	III	IV
S_c/S_L [-]	3.09	1.91	1.97	1.91
A_f/A_0 [-]	1.65	1.19	1.18	1.19
I_0 [-]	1.87	1.61	1.67	1.61

are symmetric in experiments appear asymmetric in simulations. One possible explanation is the effect of heat losses through the walls in experiments. Here, using isothermal walls, the influence of heat losses on flame front symmetry is examined for a channel width of $h = 2.7\,\mathrm{mm}$ and two equivalence ratios, $\phi = 0.8$ and $\phi = 1.0$.

Figure 9 compares flame front shapes, defined at the

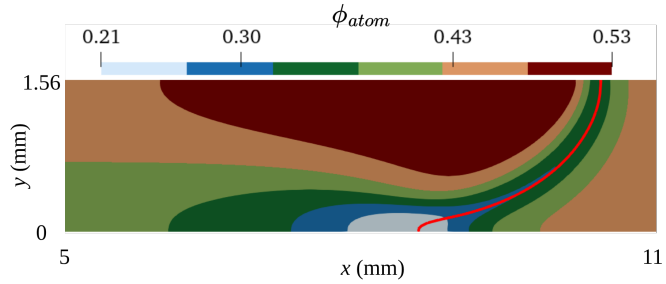

(a) Asymmetric

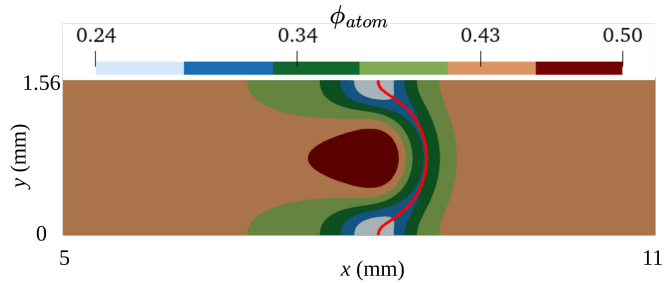

(b) Symmetric

Figure 8. $\phi = 0.43$, $h = 1.56\,\mathrm{mm}$, distribution of atom-based equivalence ratio with adiabatic walls.

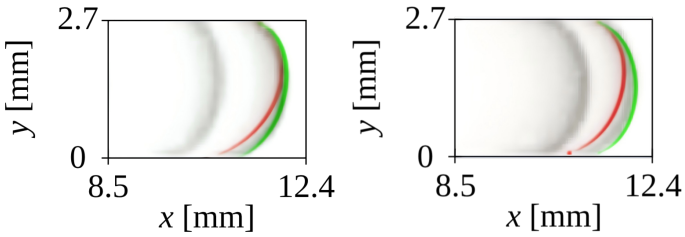

(a) $\phi = 0.8$ (b) $\phi = 1.0$

Figure 9. Flame front isosurfaces at maximum density gradient for $\phi = 0.8$ (left) and $\phi = 1.0$ (right), with $h = 2.7\,\mathrm{mm}$, grey lines stand for experimental observations, and red/green curves stand for simulations with adiabatic/isothermal walls.

maximum density gradient, with experimental data. The inclusion of heat losses shortens the flame front and can destabilize asymmetric flames into symmetric shapes (as observed for $\phi = 1.0$). This behavior may be related to the lower stability of the asymmetric flame at $\phi = 1.0$ compared to $\phi = 0.8$ for $h = 2.7\,\mathrm{mm}$, as noted in [10].

4 Conclusion

This study applied an H radical recombination model to solve abnormal near-wall "explosion" of heat release rate, which is commonly observed near cold walls when using detailed chemical mechanisms. This model is validated using canonical flame-wall interaction configurations, including head-on quenching for stoichiometric H_2/O_2 mixtures and side-wall quenching for H_2/air flames. The results of HOQ case confirm that the H radical is the dominant contributor to the abnormal near-wall heat release behavior, and demonstrate that selective H recombination provides a physically consistent and mass-conserving modeling approach. Moreover, this model introduces negligible additional computational cost (approximately 2%), as it is directly implemented as a boundary condition.

The flame propagation speed is well recovered with the proposed model in the SWQ case by comparing with experiments. Furthermore, the influence of wall heat losses on flame stability and symmetry was then investigated at larger channel widths, where multiple steady flame solutions are known to exist under adiabatic wall conditions. For $\phi = 0.43$ and $h = 1.56$ mm, both an asymmetric half-hump flame and a symmetric one-hump flame were examined. The results show that the asymmetric solution becomes unstable in the presence of wall heat losses, whereas the symmetric flame remains stable and only weakly affected at this width. At even larger channel widths, where stable asymmetric one-hump flames exist under adiabatic conditions, the introduction of heat losses consistently promotes a transition toward symmetric flame configurations and recovers the flame shape observed from experiments. These findings provide a plausible explanation for discrepancies in flame symmetry observed between adiabatic numerical simulations and experimental measurements in confined hydrogen combustion systems. Overall, this work provides a validated and computationally efficient modeling strategy for treating flame-wall interaction and heat losses in premixed hydrogen combustion. By improving the physical fidelity of numerical predictions in confined and wall-bounded configurations, the present findings contribute to safer and more reliable design and analysis of hydrogen-based energy systems operating under carbon-neutral combustion concepts.

Data Availability Statement

Data will be made available on request.

Funding

This work was supported by the IMI Institut Mécanique et Ingénierie funding and the ECOSAFE ANR project under Grant ANR-21-CE05-0028.

Access to high-performance computing resources was provided by the Centre de Calcul Intensif d'Aix-Marseille and GENCI-TGCC/CINES under Grant A0152B11951.

Conflicts of Interest

The authors declare no conflicts of interest.

AI Use Statement

The authors declare that no generative AI was used in the preparation of this manuscript.

Ethical Approval and Consent to Participate

Not applicable.

References

[1] Poinsot, T., & Veynante, D. (2005). *Theoretical and numerical combustion*. RT Edwards, Inc.

[2] Popp, P., & Baum, M. (1997). Analysis of wall heat fluxes, reaction mechanisms, and unburnt hydrocarbons during the head-on quenching of a laminar methane flame. *Combustion and Flame, 108*(3), 327-348. [CrossRef]

[3] Dabireau, F., Cuenot, B., Vermorel, O., & Poinsot, T. (2003). Interaction of flames of H2+ O2 with inert walls. *Combustion and flame, 135*(1-2), 123-133. [CrossRef]

[4] Peters, N., & Warnatz, J. (2013). *Numerical methods in laminar flame propagation: A GAMM-Workshop*. Springer-Verlag.

[5] Liu, J., Yu, R., Ma, B., & Tang, C. (2020). On the second explosion limits of hydrogen, methane, ethane, and propane. *ACS omega, 5*(30), 19268-19276. [CrossRef]

[6] Li, J., Liang, W., Chen, J., Han, W., & Law, C. K. (2022). Role of surface reactions in hydrogen–oxygen explosion limits. *Energy & Fuels, 36*(20), 12729-12736. [CrossRef]

[7] De Nardi, L., Douasbin, Q., Vermorel, O., & Poinsot, T. (2024). Infinitely fast heterogeneous catalysis model for premixed hydrogen flame-wall interaction. *Combustion and flame, 261*, 113328. [CrossRef]

[8] Dejoan, A., Jiménez, C., & Kurdyumov, V. N. (2019). Critical conditions for non-symmetric flame propagation in narrow channels: Influence of the flow rate, the thermal expansion, the Lewis number and heat-losses. *Combustion and Flame, 209*, 430-440. [CrossRef]

[9] Bioche, K., Vervisch, L., & Ribert, G. (2018). Premixed flame–wall interaction in a narrow channel: impact of wall thermal conductivity and heat losses. *Journal of Fluid Mechanics, 856*, 5-35. [CrossRef]

[10] Chen, Z., Ballossier, Y., Zhao, S., Denet, B., Almarcha, C., & Boivin, P. (2025). Study on symmetric/asymmetric hydrogen flame shapes in the thickness of a Hele-Shaw burner. *Combustion and Flame, 277*, 114208. [CrossRef]

[11] Boivin, P., Tayyab, M., & Zhao, S. (2021). Benchmarking a lattice-Boltzmann solver for reactive flows: Is the method worth the effort for combustion?. *Physics of Fluids, 33*(7). [CrossRef]

[12] Chen, Z., Zhao, S., Denet, B., Almarcha, C., & Boivin, P. (2025). A three-dimensional study on premixed flame propagation in narrow channels considering hydrodynamic and thermodiffusive instabilities. *Combustion and Flame, 281*, 114392. [CrossRef]

[13] Farag, G., Zhao, S., Coratger, T., Boivin, P., Chiavassa, G., & Sagaut, P. (2020). A pressure-based regularized lattice-Boltzmann method for the simulation of compressible flows. *Physics of Fluids, 32*(6). [CrossRef]

[14] Boivin, P., Jiménez, C., Sánchez, A. L., & Williams, F. A. (2011). An explicit reduced mechanism for H2–air combustion. *Proceedings of the Combustion Institute, 33*(1), 517-523. [CrossRef]

[15] Boivin, P., Dauptain, A., Jiménez, C., & Cuenot, B. (2012). Simulation of a supersonic hydrogen–air autoignition-stabilized flame using reduced chemistry. *Combustion and Flame, 159*(4), 1779-1790. [CrossRef]

[16] CERFACS. (n.d.). *Hydrogen mechanism (Cantera chemical mechanisms)*. Cantera CERFACS. https://www.cerfacs.fr/cantera/mechanisms/hydro.php

[17] Ballossier, Y., Boivin, P., & Almarcha, C. (2024). Three dimensional shapes of hydrogen-air flames within millimetric Hele Shaw cells. *International Journal of Hydrogen Energy, 60*, 333-341. [CrossRef]

Ziyin Chen received the Ph.D. degree from Aix Marseille University, Marseille, France, in 2026. He/She is currently with Aix Marseille Univ, CNRS, Centrale Marseille, M2P2, Marseille, France. (Email: ziyin.chen@univ-amu.fr)

Yuxi Mai received the Ph.D. degree from Northwestern Polytechnical University, Xi'an, China, in 2026. He/She is currently with the School of Management, Northwestern Polytechnical University, Xi'an, China. (Email: maiyuxi@mail.nwpu.edu.cn)